Nonequilibrium thermodynamics of glycolytic traveling wave: Benjamin-Feir instability

Premashis Kumar and Gautam Gangopadhyay*

S. N. Bose National Centre For Basic Sciences, Block-JD, Sector-III, Salt Lake, Kolkata 700 106, India

(Received 13 April 2021; accepted 8 July 2021; published 30 July 2021)

Evolution of the nonequilibrium thermodynamic entities corresponding to dynamics of the Hopf instabilities and traveling waves at a nonequilibrium steady state of a spatially extended glycolysis model is assessed here by implementing an analytically tractable scheme incorporating a complex Ginzburg-Landau equation (CGLE). In the presence of self and cross diffusion, a more general amplitude equation exploiting the multiscale Krylov-Bogoliubov averaging method serves as an essential tool to reveal the various dynamical instability criteria, especially Benjamin-Feir (BF) instability, to estimate the corresponding nonlinear dispersion relation of the traveling wave pattern. The critical control parameter, wave-number selection criteria, and magnitude of the complex amplitude for traveling waves are modified by self- and cross-diffusion coefficients within the oscillatory regime, and their variabilities are exhibited against the amplitude equation. Unlike the traveling waves, a low-amplitude broad region appears for the Hopf instability in the concentration dynamics as the system phase passes through minima during its variation with the control parameter. The total entropy production rate of the uniform Hopf oscillation and glycolysis wave not only qualitatively reflects the global dynamics of concentrations of intermediate species but almost quantitatively. Despite the crucial role of diffusion in generating and shaping the traveling waves, the diffusive part of the entropy production rate has a negligible contribution to the system's total entropy production rate. The Hopf instability shows a more complex and colossal change in the energy profile of the open nonlinear system than in the traveling waves. A detailed analysis of BF instability shows a contrary nature of the semigrand Gibbs free energy with discrete and continuous wave numbers for the traveling wave. We hope the Hopf and traveling wave pattern around the BF instability in terms of energetics and dissipation will open up new applications of such dynamical phenomena.

DOI: 10.1103/PhysRevE.104.014221

I. INTRODUCTION

Oscillation is a ubiquitous phenomenon in a living system [1–3], starting from cellular rhythms [4–6], oscillation in single enzyme systems [7], to glycolytic oscillation in a cell [8,9] with a diverse oscillatory pattern from different origin but with a universal underlying principle. Glycolysis, a crucial energy-generating pathway of the metabolism in a living system, involves a complex chemical reaction network. From simple nonlinear models [10,11] to sophisticated complex models [12–14], several theoretical schemes have been proposed to capture the temporal and spatial oscillatory behavior of glycolysis. However, the intricacy of the sophisticated glycolysis model hinders the investigation of any particular mechanism within a specific regime. Therefore, in the spirit of simplicity and clarity, we have chosen the two-variable Selkov model extended by diffusion, which provides scope for studying the vital dynamical features and elaborating them from the theoretical ground [15,16]. From the kinetic picture of glycolysis to the Selkov equation, obscurity arises with the consideration of many irreversible states. Here we have concentrated on the reversible kinetics of the Selkov model as an open system with Rayleigh oscillator form to study nonequilibrium steady-state (NESS) [17] phenomena.

The generation of traveling waves from glycolytic activity in the diffusive layer exploiting the yeast extracts in an open spatial reactor is previously demonstrated [18,19] experimentally. On the other hand, an amplitude equation [3,20] in the presence of diffusive coupling is utilized to explain the appearance of inward rotating spiral waves in glycolysis [21,22]. However, in the previous study [16] of the Selkov model involving an amplitude equation, either diffusion coefficients are taken equally in magnitude for analytic investigation or their contribution is neglected. In our amplitude equation consideration, all the diffusion coefficients (self and cross) are present and can take any range of values. In this aspect, our findings related to the amplitude equation would enable one with more flexibility in exploring and studying various standard glycolysis model performance, generic features, and robustness. For the Selkov glycolysis model, inhomogeneous control parameter flux [16,23] or periodic substrate influx [24] has been often considered to investigate various rich features such as phase reversal, chaotic oscillation, or oscillation entrainment within the oscillatory regime. However, we have considered the homogeneous concentration of the control parameter in this report. Therefore features that appear in homogenous Hopf oscillation or traveling waves are solely due to uniform chemostatted species concentration and diffusion coefficients.

The main focus of investigating glycolysis waves was limited to controlling the spatiotemporal pattern [2,3], recognizing the vital influential factors of the oscillating behavior

*gautam@bose.res.in

and entrainment of intrinsic glycolytic oscillations until now. However, the role of glycolysis waves in processing and spreading biological information [25–27], and thus dictating the coordination among events in the system, seeks to address the questions related to entropic cost, energetics, or efficiency of the wave. In this report we have investigated the evolution of nonequilibrium thermodynamic entities corresponding to the uniform oscillation and traveling waves in a simple glycolysis model system of finite size. This thermodynamic description will help to understand any nonlinear system containing limit cycles or waves on a fundamental level. Furthermore, our general analysis of the canonical complex Ginzburg-Landau equation (CGLE) for the extended reaction-diffusion systems in the presence of both self and cross diffusion [28] in this report will shed light on how the different instabilities dictated by the coefficients of amplitude equation to imprint their signatures on the evolution of the thermodynamic entities near Hopf instability point at NESS.

The layout of the report is as follows. In Sec. II we have discussed the reaction dynamics of the Selkov model and its reversible equivalent version. The reaction-diffusion form of the glycolytic model and its linear stability analysis are provided in the next section. In Sec. IV we have derived the CGLE equation using the Krylov-Bogolyubov (KB) method and then separate the magnitude and the phase dynamics. In Sec. V the concentration fields are obtained by combining analytical results in previous sections. Entropy production rate and nonequilibrium Gibbs free energy are formulated for the reaction-diffusion system in Sec. VI. We have provided numerical results and discussions in Sec. VII. Finally, the paper is concluded in Sec. VIII.

II. SIMPLE GLYCOLYSIS MODEL: FROM KINETIC SELKOV MODEL TO REVERSIBLE MODEL

In this section we derive simplified partial differential equation forms of the simple glycolytic models from their standard chemical reaction networks. The simplified system will be utilized for linear stability analysis and amplitude equation formulation in later sections of the report.

A. Kinetic Selkov model

E. E. Selkov proposed a simple kinetic model of glycolysis [10] that exhibits periodic oscillation for a specific range of parameters. The Selkov model contains the following sequence of chemical reactions:

$$\begin{aligned}
\rho = 1: &\quad \mathrm{S_1} + \mathrm{ES_2^2} \underset{\mathrm{k^{\cdot}\text{-}1}}{\overset{\mathrm{k^{\cdot}1}}{\rightleftharpoons}} \mathrm{S_1ES_2^2} \\
\rho = 2: &\quad \mathrm{S_1ES_2^2} \xrightarrow{\mathrm{k^{\cdot}2}} \mathrm{ES_2^2} + \mathrm{S_2} \\
\rho = 3: &\quad 2\,\mathrm{S_2} + \mathrm{E} \underset{\mathrm{k^{\cdot}\text{-}3}}{\overset{\mathrm{k^{\cdot}3}}{\rightleftharpoons}} \mathrm{ES_2^2}
\end{aligned} \tag{1}$$

where $'\rho'$ is a reaction step label. The substrate $S_1(ATP)$ is supplied at constant rate z_1, and the product $S_2(ADP)$ is removed at a rate v_2. The free enzyme $E(phosphofructokinase)$ is initially inactive and becomes active only after combining with the product S_2 to form a complex ES_2^2. It should be noted that a chemical reaction corresponding to $\rho = 2$ here generates the product, $S_2(ADP)$, irreversibly.

With the assumption that all the reverse rate constants $k_{-\rho}$ are vanishingly small (10^{-4}), and the forward reaction rate constants k_ρ are much higher than the reverse one, i.e., $k_\rho \gg k_{-\rho}$, the rate equations of concentrations of intermediate species in Eq. (1) yield

$$\begin{aligned}
\dot{x_1} &= (k_1 + k_2)x_2 - k_1 s_1 x_1 + k_3(e_0 - x_1 - x_2)s_2^2 - k_{-3}x_1 \\
\dot{x_2} &= k_1 s_1 x_1 - (k_{-1} + k_2)x_2,
\end{aligned} \tag{2}$$

where concentrations of the species are denoted by

$$x_1 = \left[ES_2^2\right], x_2 = \left[S_1 ES_2^2\right], s_1 = [S_1], s_2 = [S_2].$$

The steady-state solution of Eq. (2) is

$$x_1^{s.s.} = \frac{e_0 k_3 s_2^2 [k_2 + k_{-1}]}{S}, \tag{3a}$$

$$x_2^{s.s.} = \frac{e_0 k_3 k_1 s_1 s_2^2}{S}, \tag{3b}$$

where $S = (k_1 s_1 + k_3 s_2^2 + k_{-3})(k_2 + k_{-1}) - (k_{-1} + k_2 - k_3 s_2)(k_1 s_1)$. After rearranging Eqs. (3a) and (3b) we arrive at the following form:

$$x_1^{s.s.} = \frac{e_0 \zeta_2^2}{1 + \zeta_2^2(1 + \zeta_1)}, \tag{4a}$$

$$x_2^{s.s.} = \frac{e_0 \zeta_1 \zeta_2^2}{1 + \zeta_2^2(1 + \zeta_1)}, \tag{4b}$$

where $\zeta_1 = \frac{k_1}{k_{-1}+k_2} s_1$ and $\zeta_2 = \sqrt{\frac{k_3}{k_{-3}}} s_2$ are relative concentrations of substrate and product, respectively. Furthermore, we can also obtain $e^{s.s.} = \frac{e_0}{1+\zeta_2^2(1+\zeta_1)}$ by exploiting the fact that total enzyme concentration remains constant over the whole process. From Eq. (1) we can write the following dynamical equation:

$$\frac{\partial s_1}{\partial t} = z_1 - k_1 s_1 x_1 + k_{-1} x_2, \tag{5a}$$

$$\frac{\partial s_2}{\partial t} = k_2 x_2 - k_3(e_0 - x_1 - x_2)s_2^2 + k_{-3}x_1 - k_2 s_2. \tag{5b}$$

After dimensionless analysis of Eqs. (5a) and (5b), we have

$$\frac{\partial \zeta_1}{\partial \theta} = z - \left(1 + \frac{k_{-1}}{k_2}\right)\frac{\zeta_1 x_1}{e_0} + \frac{k_{-1}}{k_2}\frac{x_2}{e_0}, \tag{6a}$$

$$\frac{\partial \zeta_2}{\partial \theta} = \alpha_2\left[\frac{x_2}{e_0} - \frac{k_{-3}}{k_2}\frac{e}{e_0}\zeta_2^2 + \frac{k_{-3}}{k_2 e_0}x_1 - X_2\zeta_2\right], \tag{6b}$$

where $z = \frac{z_1}{k_2 e_0}, \theta = \frac{k_1 k_2 e_0 t}{k_{-1}+k_2}, \alpha_2 = \frac{k_2+k_{-1}}{k_1}\sqrt{\frac{k_3}{k_{-3}}}, X_2 = \frac{1}{e_0}\sqrt{\frac{k_{-3}}{k_3}}$. Now, further applying dimensionless analysis on Eq. (2), we get

$$\epsilon\frac{\partial x_1}{\partial \theta} = x_2 - x_1\zeta_1 - \frac{K_3}{K_1 + 1}\left[x_1 - \zeta_2^2 e\right], \tag{7a}$$

$$\epsilon\frac{\partial x_2}{\partial \theta} = \zeta_1 x_1 - x_2, \tag{7b}$$

where $\epsilon = \frac{k_1 k_2}{(k_{-1}+k_2)^2}, K_3 = \frac{k_{-3}}{k_2}, K_1 = \frac{k_{-1}}{k_2}$. By considering ϵ is a very small quantity, we can substitute x_1, x_2, e in Eqs. (6a)

and (6b) by their steady-state values. Thus, Eqs. (6a) and (6b) become

$$\frac{\partial \zeta_1}{\partial \theta} = z - \frac{\zeta_1 \zeta_2^2}{1 + \zeta_2^2(1+\zeta_1)}, \tag{8a}$$

$$\frac{\partial \zeta_2}{\partial \theta} = \alpha_2 \left[\frac{\zeta_1 \zeta_2^2}{1 + \zeta_2^2(1+\zeta_1)} - X_2 \zeta_2 \right]. \tag{8b}$$

For further simplification we introduce the rescaled quantities $\tau = X_2^2 z^{-2}\theta$, $x = X_2^{-1} z \alpha_2 \zeta_1$, $y = X_2^{-1} z \zeta_2$, $\nu = X_2^{-3} z^4 \alpha_2$, $\omega = X_2^{-1} z^2 \alpha_2$, $\kappa = z X_2^{-1} \alpha_2$ in Eqs. (8a) and (8b), and obtain the following system:

$$\frac{\partial x}{\partial \tau} = \nu - \frac{x y^2}{1 + \frac{z}{\nu} y^2 (\kappa + x)}, \tag{9a}$$

$$\frac{\partial y}{\partial \tau} = \frac{x y^2}{1 + \frac{z}{\nu} y^2 (\kappa + x)} - \omega y. \tag{9b}$$

Due to slow glycolytic flux during self-oscillation, i.e., for $z \ll 1$, we can write $1 + \frac{z}{\nu} y^2 (\kappa + x) = 1$. Finally, the simplified form of the Selkov model system can be written as

$$\begin{aligned} \frac{\partial x}{\partial \tau} &= \nu - x y^2, \\ \frac{\partial y}{\partial \tau} &= x y^2 - \omega y. \end{aligned} \tag{10}$$

B. Chemostatted Selkov model

For the nonequilibrium thermodynamic representation of the chemical reaction network, all the elementary chemical reactions must be reversible. However, as mentioned earlier, the elementary reaction of $\rho = 2$ in Eq. (1) in the Selkov scheme is irreversible. An equivalent, completely reversible description based on the Selkov model can be written as [29]

$$\begin{aligned} \rho = 1: &\quad \mathrm{A} \underset{\mathrm{k'\text{-}1}}{\overset{\mathrm{k'1}}{\rightleftharpoons}} \mathrm{S} \\ \rho = 2: &\quad \mathrm{S} + 2\,\mathrm{P} \underset{\mathrm{k'\text{-}2}}{\overset{\mathrm{k'2}}{\rightleftharpoons}} 3\,\mathrm{P} \\ \rho = 3: &\quad \mathrm{P} \underset{\mathrm{k'\text{-}3}}{\overset{\mathrm{k'3}}{\rightleftharpoons}} \mathrm{B} \end{aligned} \tag{11}$$

where S and P are the ATP and ADP concentrations, respectively. This reversible reaction network would be convenient in connecting kinetic and thermodynamic descriptions. Here $\{S, P\} \in I$ are two intermediate species having dynamic concentration, and $\{A, B\} \in C$ are externally controllable chemostatted species. Considering that reverse reaction rates are very small relative to the forward reaction rates, we can write the dynamical equation of Eq. (11) as

$$\begin{aligned} \frac{\partial s}{\partial t} &= k_1 a - k_2 s p^2, \\ \frac{\partial p}{\partial t} &= k_2 s p^2 - k_3 p. \end{aligned} \tag{12}$$

By introducing the scaled variables $\tau = \frac{k_2 t}{c_1^2}$, $\nu = \frac{c_1^3 k_1 a}{k_2}$, $x = c_1 s$, $y = c_1 p$, $\omega = \frac{c_1^2 k_3}{k_2}$ in Eq. (12), we would have the same set of equations as in Eq. (10). Here c_1 is an arbitrary constant. We would use the parameter ν as the control parameter of the system, keeping another parameter ω at a fixed value.

III. DYNAMICAL STABILITY OF THE SYSTEM WITH DIFFUSION

When the spatial aspect of the system is not considered, we can only have Hopf instability with uniform oscillation with wave number $q = 0$ in the model. In a more general case with a nonzero finite wave number, the reaction-diffusion model of glycolysis also admits traveling waves.

A unique steady-state value of Eq. (10) that satisfies $\dot{x} = \dot{y} = 0$ is $x_0 = \frac{\omega^2}{\nu}$, $y_0 = \frac{\nu}{\omega}$. For linear stability analysis at the steady-state value (x_0, y_0), one needs to consider the Jacobian matrix of the model,

$$\mathcal{J} = \begin{pmatrix} -{y_0}^2 & -2x_0 y_0 \\ {y_0}^2 & 2x_0 y_0 - \omega \end{pmatrix}. \tag{13}$$

Elements of the Jacobian matrix $\mathcal{J}$ are the following:

$J_{11} = -{y_0}^2$, $J_{12} = -2x_0 y_0$, $J_{21} = {y_0}^2$, $J_{22} = 2x_0 y_0 - \omega$.

Determinant and trace of the Jacobian, $\mathcal{J}$, are $\det(\mathcal{J}) = \frac{\nu^2}{\omega}$ and $\mathrm{Tr}(\mathcal{J}) = \omega - (\frac{\nu}{\omega})^2$, respectively. Eigenvalues, λ of $\mathcal{J}$ are given by the characteristic equation, $\lambda^2 - \mathrm{Tr}(\mathcal{J})\lambda + \det(\mathcal{J}) = 0$. Hence eigenvalues in terms of determinant and trace are

$$\lambda_\pm = \frac{\mathrm{Tr}(\mathcal{J}) \pm \sqrt{\mathrm{Tr}(\mathcal{J})^2 - 4\det(\mathcal{J})}}{2}. \tag{14}$$

As chemical parameters are real quantities, eigenvalues of the system at stable steady-state are the complex conjugate pair $\lambda_\pm = \lambda_r \pm i\lambda_i$. At the onset of Hopf instability, $\mathrm{Tr}(\mathcal{J}) = 0$, i.e., $J_{11} + J_{22} = 0$, and it leads to a critical value of the control parameter as $\nu_{cH} = \omega\sqrt{\omega}$. Therefore, at the onset of the Hopf instability, the determinant is $\det(\mathcal{J}) = \omega^2$ and eigenvalues are $\lambda_\pm = \pm i\omega$. The critical frequency of the Hopf instability f_{cH} will be the imaginary part of the eigenvalue λ at the onset of instability, and hence the period of the limit cycle near the onset of instability ν_{cH} is approximately $T = \frac{2\pi}{f_{cH}}$, where $f_{cH} = \omega$. Now the critical eigenvector U_{cH}, corresponding to the eigenvalue $\lambda = i\omega$ at the onset of Hopf instability, is

$$U_{cH} = \begin{pmatrix} 1 - i \\ -1 \end{pmatrix}. \tag{15}$$

Now in the presence of diffusion, the reaction-diffusion equation of the Selkov model in one spatial dimension $r \in [0, l]$ can be expressed from Eq. (10) as

$$\begin{aligned} \frac{\partial x}{\partial \tau} &= \nu - x y^2 + D_{11} x_{rr} + D_{12} y_{rr}, \\ \frac{\partial y}{\partial \tau} &= x y^2 - \omega y + D_{21} x_{rr} + D_{22} y_{rr}, \end{aligned} \tag{16}$$

in which D_{11}, D_{22} are self-diffusion coefficients corresponding to intermediate species x and y, respectively, and D_{12}, D_{21} are cross-diffusion coefficients of x and y. Diffusion coefficients can have concentration dependence. However, we have considered here constant self- and cross-diffusion coefficients for simplicity.

In the presence of diffusion, the Jacobian $\mathcal{J}$ becomes

$$\begin{aligned} \mathcal{J}_\mathcal{D} &= \mathcal{J} - q^2 \mathcal{D} \\ &= \begin{pmatrix} -{y_0}^2 & -2x_0 y_0 \\ {y_0}^2 & 2x_0 y_0 - \omega \end{pmatrix} - q^2 \begin{pmatrix} D_{11} & D_{12} \\ D_{21} & D_{22} \end{pmatrix}, \end{aligned} \tag{17}$$

where we have applied a Fourier transform $g(r,t) \to g(q,t)$, with q being the wave number. Now the trace of $\mathcal{J}_\mathcal{D}$ is $\mathrm{Tr}(\mathcal{J}_\mathcal{D}) = \mathrm{Tr}(\mathcal{J}) - q^2\mathrm{Tr}(\mathcal{D}) = \omega - (\frac{\nu}{\omega})^2 - (D_{11} + D_{22})q^2$, and the determinant of $\mathcal{J}_\mathcal{D}$ is a quadratic equation of q^2,

$$\det(\mathcal{J}_\mathcal{D}) = \det(\mathcal{D})q^4 - [D_{11}J_{22} + D_{22}J_{11} - D_{12}J_{21} - D_{21}J_{12}]q^2 + \det(\mathcal{J}), \quad (18)$$

in which $\det(\mathcal{J}) = \frac{\nu^2}{\omega}$ is the determinant of $\mathcal{J}$, and $\det(\mathcal{D})$ is the determinant of the matrix containing diffusion coefficients. The eigenvalues λ of $\mathcal{J}_\mathcal{D}$ are obtained by the characteristic equation $\lambda^2 - \mathrm{Tr}(\mathcal{J}_\mathcal{D})\lambda + \det(\mathcal{J}_\mathcal{D}) = 0$. Hence eigenvalues can be expressed only in terms of determinant and trace as

$$\lambda_\pm = \frac{\mathrm{Tr}(\mathcal{J}_\mathcal{D}) \pm \sqrt{\mathrm{Tr}(\mathcal{J}_\mathcal{D})^2 - 4\det(\mathcal{J}_\mathcal{D})}}{2}. \quad (19)$$

The stability criterion would demand both of these eigenvalues have to be negative, and thus in terms of trace and determinant, this implies $\mathrm{Tr}(\mathcal{J}_\mathcal{D}) < 0$ and $\det(\mathcal{J}_\mathcal{D}) > 0$. The existence of the traveling wave in the presence of diffusion demands that $\mathrm{Tr}(\mathcal{J}_\mathcal{D}) = 0$ and $\det(\mathcal{J}_\mathcal{D}) > 0$.

Now, exploiting the $\mathrm{Tr}(\mathcal{J}_\mathcal{D}) = 0$ condition, the critical value of the control parameter ν can be specified as

$$\nu_{ctw} = w\sqrt{w - (D_{11} + D_{22})q^2}. \quad (20)$$

The wave number q has to follow $q = \frac{2n\pi}{l}$ according to periodic boundary conditions in the finite domain of size l. Here n is an integer and specifies the number of oscillations within the region of interest. The condition $\det(\mathcal{J}_\mathcal{D}) > 0$ for generating a traveling wave imposes a restriction on the wave-number selection. Hence the wave number q in this model needs to satisfy the condition obtained from (18),

$$\det(\mathcal{D})q^4 - [D_{11} - D_{22} - D_{12} + 2D_{21}]wq^2 + w^2 > 0. \quad (21)$$

IV. AMPLITUDE EQUATION IN THE PRESENCE OF CROSS DIFFUSION

The amplitude of a dynamical system is generally a complex quantity that demonstrates features akin to the order parameter in a phase transition. We have used the KB averaging method [30] to find out the magnitude and phase dynamical equation of the extended Selkov model in the presence of both self- and cross diffusion. In this KB method, the slowly varying magnitude and phase allow us to treat the instantaneous amplitude equation and the averaged amplitude equation on an equal footing.

Initially, two new variables, i.e., the total concentration of intermediate species $z = x + y$ and total flux of $u = \nu - \omega y$, have been introduced to rewrite Eq. (10) of the Selkov model in the following form:

$$\dot{z} = u,$$
$$\dot{u} = -\omega(u - \nu) - \omega^{-2}(\omega z + u - \nu)(u - \nu)^2. \quad (22)$$

The steady-state solution of the new set of differential equations is $u_s = 0$ and $z_s = \frac{\omega^2}{\nu} + \frac{\nu}{\omega}$. From now on we use the notation t in the place of τ to denote time. Now setting up another new variable as $\zeta = z - z_s$ will shift the fixed point of the system to the origin. With the aid of u and ζ it is possible to represent (22) as a single second-order equation akin to the generalized Rayleigh equation [23,31,32],

$$\ddot{\zeta} + \Omega^2\zeta = \lambda\left[2(1 + c_1u - c_2u^2)u - \frac{\Omega^2}{\lambda}(\nu^{-2}u^2 - 2\nu^{-1}u)\zeta\right], \quad (23)$$

where $\Omega = \frac{\nu}{\sqrt{\omega}}$, $\lambda = \frac{\omega - \omega^{-2}\nu^2}{2}$, $c_1 = \frac{(2\omega^{-2}\nu - \frac{\omega}{\nu})}{2\lambda}$, $c_2 = \frac{\omega^{-2}}{2\lambda}$. By inserting $2(1 + c_1u - c_2u^2)u - \frac{\Omega^2}{\lambda}(\nu^{-2}u^2 - 2\nu^{-1}u)\zeta = h$ in Eq. (23), we obtain

$$\ddot{\zeta} + \Omega^2\zeta = \lambda h. \quad (24)$$

Now for the reaction-diffusion representation of the Selkov model, Eq. (16) comprising of both self- and cross-diffusion coefficients, we can extend Eq. (24) in the following way:

$$\ddot{\zeta} + \Omega^2\zeta = \lambda h + (D_{22} + D_{12} - D_{11} - D_{21})\dot{u}_{rr} + (D_{22} + D_{12})\dot{\zeta}_{rr} + (D_{11} - D_{12})u_{rr} - D_{12}\zeta_{rr}. \quad (25)$$

For λ being infinitesimal, Eq. (25) would accept simple harmonic-function-like solutions,

$$\zeta(r,t) = \mathcal{A}(r,t)\cos[\Omega t + \phi(r,t)], \quad (26a)$$
$$u(r,t) = \dot{\zeta}(r,t) = -\Omega\mathcal{A}(r,t)\sin[\Omega t + \phi(r,t)], \quad (26b)$$

with slowly varying amplitude $\mathcal{A}$ and phase ϕ during fast oscillations. Finally, with the aid of Eq. (26a) and (26b), we acquire the dynamical equations of amplitude and phase, respectively as,

$$\dot{\mathcal{A}} = -\frac{1}{\Omega}\left[\lambda h - \Omega^2\left(D_{22} + D_{12} + \frac{D_{12}}{\Omega^2} - D_{11} - D_{21}\right)\zeta_{rr} + (D_{22} + D_{11})u_{rr}\right]\sin(\Omega t + \phi), \quad (27)$$

$$\dot{\Phi} = \frac{1}{\Omega\mathcal{A}}\left[\lambda h - \Omega^2\left(D_{22} + D_{12} + \frac{D_{12}}{\Omega^2} - D_{11} - D_{21}\right)\zeta_{rr} + (D_{22} + D_{11})u_{rr}\right]\cos(\Omega t + \phi). \quad (28)$$

Now by taking the average, amplitude and phase equations of the Selkov reaction-diffusion model in the presence of cross diffusion are obtained as

$$\dot{\mathcal{A}} = \mathcal{A}\lambda - p_1\frac{3\lambda c_2\Omega^2}{4}A^3 - \frac{\Omega}{2}\left(D_{22} + D_{12} + \frac{D_{12}}{\Omega^2} - D_{11} - D_{21}\right)(2\mathcal{A}_r\phi_r + \phi_{rr}\mathcal{A}) + \frac{(D_{11} + D_{22})}{2}(\mathcal{A}_{rr} - \mathcal{A}\phi_r^2), \quad (29a)$$

$$\dot{\Phi} = -p_2\frac{\Omega^3}{8\nu^2}\mathcal{A}^2 - \frac{(D_{11} + D_{22})}{2}\left(\frac{2\mathcal{A}_r\phi_r}{\mathcal{A}} + \phi_{rr}\right) - \frac{\Omega}{2}\left(D_{22} + D_{12} + \frac{D_{12}}{\Omega^2} - D_{11} - D_{21}\right)\left(\frac{\mathcal{A}_{rr}}{\mathcal{A}} - \phi_r^2\right). \quad (29b)$$

Here, correction factors $p_1 = \frac{c_2}{c_1}$ and $p_2 = \frac{2c_1}{vc_2}$ are introduced in Eqs. (29a) and (29b) to include the modification in radius and phase of the cycle owing to unidirectional acceleration from the unstable steady state [16].

A. Complex Ginzburg-Landau equation near Hopf onset: Amplitude and phase equations

Near the onset of Hopf instability, the lowest-order amplitude equation, the CGLE [3,20], properly reflects the dynamics of the partially extended nonlinear oscillatory models. The unscaled form of CGLE can be represented as

$$\frac{\partial Z}{\partial t} = \lambda Z - (\beta_r - i\beta_i)|Z|^2 Z + (\alpha_r + i\alpha_i)\partial_r^2 Z. \tag{30}$$

Assuming the same velocity for all the traveling waves and introducing a comoving coordinate as $r = r - velocity \times t$, we can utilize the same amplitude equation of the form of Eq. (30) for the traveling waves.

By inserting $Z = \mathcal{A}\exp(i\phi)$ in Eq. (30) and separating real and imaginary parts we obtain

$$\frac{\partial \mathcal{A}}{\partial t} = \lambda\mathcal{A} - \beta_r\mathcal{A}^3 - \alpha_i(2\mathcal{A}_r\phi_r + \phi_{rr}\mathcal{A}) + \alpha_r\left(\mathcal{A}_{rr} - \mathcal{A}\phi_r^2\right), \tag{31a}$$

$$\frac{\partial \phi}{\partial t} = \beta_i\mathcal{A}^2 + \alpha_r\left(\frac{2\mathcal{A}_r\phi_r}{\mathcal{A}} + \phi_{rr}\right) + \alpha_i\left(\frac{\mathcal{A}_{rr}}{\mathcal{A}} - \phi_r^2\right). \tag{31b}$$

Comparing amplitude and phase Eqs. (31a) and (31b) deduced from CGLE with Eqs. (29a) and (29b) derived by the KB method, we get the following coefficients: $\beta_r = p_1\frac{3\lambda c_2\Omega^2}{4}$, $\beta_i = -p_2\frac{\Omega^3}{8v^2}$, $\alpha_r = -\frac{(D_{11}+D_{22})}{2}$, $\alpha_i = -\frac{\Omega}{2}(D_{22} + D_{12} + \frac{D_{12}}{\Omega^2} - D_{11} - D_{21})$. With the help of the scaled variables $\mathcal{A} = \frac{\mathcal{A}}{\sqrt{\beta_r}}$ and $r = \frac{r}{\sqrt{\alpha_r}}$, we can represent Eqs. (31a) and (31b) as

$$\frac{\partial \mathcal{A}}{\partial t} = \lambda\mathcal{A} - \mathcal{A}^3 - \alpha(2\mathcal{A}_r\phi_r + \phi_{rr}\mathcal{A}) + \left(\mathcal{A}_{rr} - \mathcal{A}\phi_r^2\right), \tag{32a}$$

$$\frac{\partial \phi}{\partial t} = \beta\mathcal{A}^2 + \left(\frac{2\mathcal{A}_r\phi_r}{\mathcal{A}} + \phi_{rr}\right) + \alpha\left(\frac{\mathcal{A}_{rr}}{\mathcal{A}} - \phi_r^2\right), \tag{32b}$$

and the corresponding normal form of CGLE [3,33,34] in the spatially extended system as

$$\frac{\partial Z}{\partial t} = \lambda Z - (1 - i\beta)|Z|^2 Z + (1 + i\alpha)\partial_r^2 Z. \tag{33}$$

Coefficients in the normal form of CGLE are given by $\alpha = \frac{\alpha_i}{\alpha_r} = \frac{\Omega(D_{22}+D_{12}+\frac{D_{12}}{\Omega^2}-D_{11}-D_{21})}{(D_{11}+D_{22})}$ and $\beta = \frac{\beta_i}{\beta_r} = -\frac{p_2}{p_1}\frac{\sqrt{\omega}\omega}{3v}$. In the case of Hopf instability, it is apparent that only the coefficient α explicitly depends on both the self- and cross-diffusion terms.

For large r, the normal form of the CGLE, Eq. (33), has an asymptotic solution of a simple plane wave for nonlinear oscillations,

$$Z = \mathcal{A}\exp i(\omega_0 t + qr), \tag{34}$$

where ω_0 is the shift in frequency from the critical frequency ω_{cH}. Here q is a unique wave number selected by the unique spiral frequency. With the help of Eq. (34), we obtain from Eq. (33)

$$\mathcal{A}^2 = \lambda - q^2, \tag{35a}$$

$$\omega_0 = \omega_q - \omega_{cH} = \beta\mathcal{A}^2 - \alpha q^2 = \beta\lambda - (\beta + \alpha)q^2. \tag{35b}$$

Here the bulk frequency for the system or the frequency of uniform oscillation is obtained by inserting $q = q_{cH} = 0$ in (35b). In general, the phase and group velocities can be expressed by $v_p = \frac{\omega_q}{q}$ and $v_g = \frac{\partial\omega_q}{\partial q} = -2(\beta + \alpha)q$, respectively, and they can have different sign.

For slow time variation of amplitude, we can set $\mathcal{A}$ to its steady-state variation. Therefore we can write the following from Eq. (32a):

$$\mathcal{A}^2 = \lambda - \alpha\left(\frac{2\mathcal{A}_r\phi_r}{\mathcal{A}} + \phi_{rr}\right) + \left(\frac{\mathcal{A}_{rr}}{\mathcal{A}} - \phi_r^2\right). \tag{36}$$

The phase dynamical equation, Eq. (32b), contains the space derivatives of $\mathcal{A}$, and due to long-range phase variation we would remove the higher space derivatives of $\mathcal{A}$ in the final equation. Thus the steady-state amplitude, Eq. (36), can be simplified to

$$\mathcal{A}^2 = \lambda - \alpha\phi_{rr} - \phi_r^2. \tag{37}$$

By inserting Eq. (37) into Eq. (32b), we obtain the nonlinear phase dynamical equation as

$$\frac{\partial \phi}{\partial t} = \beta\lambda + (1 - \alpha\beta)\phi_{rr} - (\alpha + \beta)\phi_r^2. \tag{38}$$

Now introducing the new phase variable, $\psi = \phi - \beta\lambda t$, we acquire from (38)

$$\frac{\partial \psi}{\partial t} = (1 - \alpha\beta)\psi_{rr} - (\alpha + \beta)\psi_r^2. \tag{39}$$

The exchange between the inward and outward rotating spiral is associated with the criterion $(\alpha + \beta) < 0$, whereas the Newell criterion, $(1 - \alpha\beta) < 0$, gives rise to the Benjamin-Feir (BF) instability [3,35] from the uniform oscillation. The BF instability, a long-wave sideband instability, was first identified in deep-water waves [35]. Due to the onset of BF instability, the wave number and frequency of a previously uniform traveling wave become irregular.

Now with the aid of derivation with respect to space and setting $\psi_r = u$, we obtain the following equation similar to the Burger's equation form (39):

$$\frac{\partial u}{\partial t} = (1 - \alpha\beta)u_{rr} - (\alpha + \beta)2uu_r. \tag{40}$$

Application of the Cole-Hopf transformation, $\psi = -[\frac{1-\alpha\beta}{\alpha+\beta}]\ln\chi$, to Eq. (39) will transform it into a linear equation:

$$\frac{\partial \chi}{\partial t} = (1 - \alpha\beta)\chi_{rr}. \tag{41}$$

As phase is a real variable, the trial solution of the linear dynamical equation, Eq. (41), can be considered as $\chi = G(t)\exp(\alpha + \beta)qr$, and inserting the trial solution into Eq. (41), we would have $G(t) = G_0\exp(1 - \alpha\beta)(\alpha + \beta)^2q^2t$. Therefore a simple solution to Eq. (41) is $\chi = G_0\exp[(1 - \alpha\beta)(\alpha + \beta)^2q^2t + (\alpha + \beta)qr]$.

Accordingly, the expression of the phase of the system is

$$\phi = \beta\lambda t - \frac{1-\alpha\beta}{\alpha+\beta}[\ln G_0 + (1-\alpha\beta)(\alpha+\beta)^2 q^2 t + (\alpha+\beta)qr]. \tag{42}$$

It should be noted that modification of the system's frequency will lead to the change of wave number, q, according to the nonlinear dispersion relation in Eq. (35b).

B. Stability of the plane wave

To test the stability of the asymptotic plane wave solution of the CGLE, we can afford a small perturbation about the nonlinear wave state. Thus the perturbed plane wave would have the following form:

$$Z = (\mathcal{A} + A_{\rm per}) \exp i(qr + \omega_0 t). \tag{43}$$

Here $A_{\rm per}$ can be expressed in terms of complex growth rate, σ, in the following way:

$$A_{\rm per} = A_+ \exp(iKr + \sigma t) + \tilde{A_-} \exp(-iKr + \tilde{\sigma} t), \tag{44}$$

where $\tilde{A}$ and $\tilde{\sigma}$ are the complex conjugation of A and σ, and K corresponds to different perturbation modes. Now, inserting Eq. (43) into Eq. (33) and neglecting the higher order of the perturbation, we arrive at the following equation:

$$\begin{aligned}&\frac{\partial A_{\rm per}}{\partial t} + i\omega_0(\mathcal{A} + A_{\rm per}) \\ &= \lambda(\mathcal{A} + A_{\rm per}) - (1-i\beta)(\mathcal{A}^3 + 2\mathcal{A}^2 A_{\rm per} + \mathcal{A}^2 \tilde{A}_{\rm per}) \\ &\quad + (1+i\alpha)\left[\partial_r{}^2 A_{\rm per} + 2iq\partial_r A_{\rm per} - q^2(\mathcal{A} + A_{\rm per})\right].\end{aligned} \tag{45}$$

Now substituting Eq. (44) into Eq. (45) and rearranging in terms of functions $\exp(iKr + \sigma t)$ and $\exp(-iKr + \tilde{\sigma} t)$, we have

$$\begin{aligned}&[A_+\sigma + i\omega_0 A_+ - \lambda A_+ + (1-i\beta)(2\mathcal{A}^2 A_+ + \mathcal{A}^2 A_-) \\ &\quad + (1+i\alpha)(K+q)^2 A_+] \exp(iKr + \sigma t) \\ &\quad + [\tilde{A}_-\tilde{\sigma} + i\omega_0 \tilde{A}_- - \lambda\tilde{A}_- + (1-i\beta)(2\mathcal{A}^2\tilde{A}_- + \mathcal{A}^2\tilde{A}_+) \\ &\quad + (1+i\alpha)(K-q)^2\tilde{A}_-] \exp(-iKr + \tilde{\sigma} t) \\ &\quad + i\omega_0\mathcal{A} - \lambda\mathcal{A} + (1-i\beta)\mathcal{A}^3 + (1+i\alpha)q^2\mathcal{A} \\ &= 0.\end{aligned} \tag{46}$$

Equating the coefficients of functions $\exp(iKr + \sigma t)$ and $\exp(-iKr + \tilde{\sigma} t)$ to 0, we obtain a homogeneous system comprising two linear equations:

$$[\sigma + (1-i\beta)\mathcal{A}^2 + (1+i\alpha)(K^2 + 2qK)]A_+ + (1-i\beta)\mathcal{A}^2 A_- = 0, \tag{47a}$$

$$[\sigma + (1+i\beta)\mathcal{A}^2 + (1-i\alpha)(K^2 - 2qK)]A_- + (1+i\beta)\mathcal{A}^2 A_+ = 0. \tag{47b}$$

We can represent Eq. (47a) and Eq. (47b) as

$$H\begin{pmatrix} A_+ \\ A_- \end{pmatrix} = 0\,, \tag{48}$$

where

$$H = \begin{bmatrix} \sigma + (1-i\beta)\mathcal{A}^2 \\ +(1+i\alpha)(K^2+2qK) & (1-i\beta)\mathcal{A}^2 \\ (1+i\beta)\mathcal{A}^2 & \sigma + (1+i\beta)\mathcal{A}^2 \\ & +(1-i\alpha)(K^2-2qK) \end{bmatrix}.$$

By setting $\det(H) = 0$, we can find the characteristic equation for σ and solving the characteristic equation, we get the most positive growth rate σ as

$$\sigma = -\mathcal{A}^2 - K^2 - 2i\alpha qK + \sqrt{(1+\beta^2)\mathcal{A}^4 - (\alpha K^2 - \beta\mathcal{A}^2 - 2iqK)^2}. \tag{49}$$

Now to explore the long-wavelength behavior, we have expanded Eq. (49) around $K = 0$,

$$\sigma = -2iq(\alpha+\beta)K + \left[\frac{[2q^2(1+\beta^2) + \beta\alpha\mathcal{A}^2]}{\mathcal{A}^2} - 1\right]K^2 + O(K^3). \tag{50}$$

We seek the threshold of stable wave number above which traveling waves show instability. The condition $\partial_{KK}\sigma = 0$ sets a boundary between the stable and unstable wave number. Therefore, at the onset of instability one can find

$$q^2 = \frac{\lambda(1-\alpha\beta)}{2\beta^2 - \alpha\beta + 3}. \tag{51}$$

Thus the wave number lying within the band set by Eq. (51) near the critical wave number of the Hopf instability would be the allowed wave number of the traveling wave. Unlike the equilibrium system, the wave number selection is a significant problem to be addressed in a finite system far from equilibrium [3]. We can have different wave numbers corresponding to control parameter values based on different boundary conditions, dynamical processes, perturbations, and methodologies. Here we have considered a finite system with periodic boundary conditions. The wave number q has to satisfy $q = \frac{2n\pi}{l}$, where n is an integer to fit the domain length l and periodic boundary conditions. Therefore the wave number is quantized, and we have a discrete set of possible wave numbers of the plane waves as the control parameter of the system is tuned. Now the perturbation wave number K also needs to fit in the finite domain with periodic boundary conditions, and thus we can write the allowed wave number, $q \pm K = \frac{2m\pi}{l}$. Here m is also an integer and generally $m \neq n$. The perturbation wave number can be kept at a minimum finite value by maintaining $|m - n| = 1$ near the critical wave number of the Hopf instability. Thus we obtain a discontinuous change in allowed wave numbers for the control parameter. Now within the BF instability regime, plane waves are linearly unstable. However, due to the convective nature of the instability, linearly unstable waves can hold some physical relevance. Near the onset of BF instability, q approaches zero. For $q = 0$, Eq. (49) results in the following equation:

$$\sigma_{q=0} = -\lambda - K^2 + \sqrt{\lambda^2 - \alpha^2 K^4 + 2\alpha\beta K^2\lambda}. \tag{52}$$

Now, expanding Eq. (52) for $K \to 0$ and then setting the Taylor expansion of $\sigma_{q=0}$ to zero, we arrive at the following

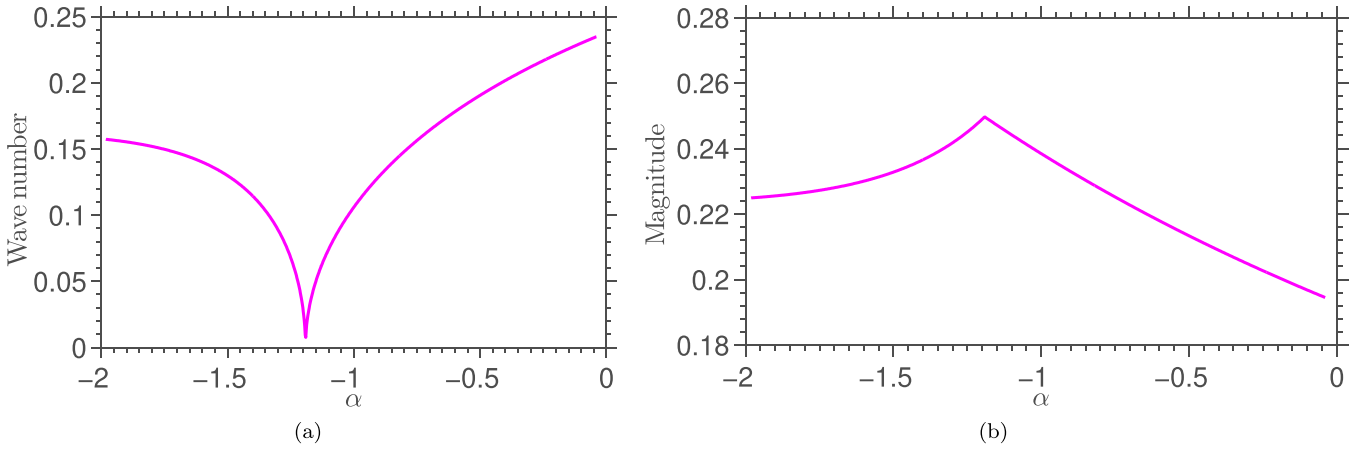

FIG. 1. Wave number vs the amplitude equation coefficient α is shown in Fig. 1(a). Figure 1(b) illustrates variation of the magnitude of the complex amplitude with respect to the same coefficient, α. Both figures are obtained by varying the cross-diffusion coefficient D_{12} from $-0.000\,01$ to -0.0005 and D_{21} from $0.000\,01$ to 0.0005 while other parameters are fixed, i.e., $D_{11} = D_{22} = 0.000\,51$, $\nu = 2.45$ and $w = 2$.

expression:

$$K_c^2 = \frac{2\lambda(\alpha\beta - 1)}{\alpha^2(1+\beta^2)}. \tag{53}$$

For the control parameter value extremely near the BF instability onset and within the BF instability regime, linearly unstable modulated waves with the discrete allowed wave numbers obtained from the band $|K| < K_c$ persist in the system. The effect of the finite domain size on the wave number selection is presented in detail in Ref. [36].

Equation (51) suggests the wave number q depends explicitly on the amplitude equation coefficients α and β. Equation (53) also shows that the K_c expression contains α and β. Now the coefficient α contains the cross-diffusion terms, so by plotting wave numbers against α in Fig. 1(a), we have shown the nature of implicit dependence of the wave number on the cross diffusion by varying both the cross-diffusion coefficients simultaneously while keeping all the other parameters, including the self-diffusion coefficients, fixed. Here the zero wave number point corresponds to the onset of the BF instability point. Therefore it is possible to enter or leave the BF instability regime by tuning only the cross-diffusion coefficients of the system. However, the continuous variation of wave number is only possible for infinite system consideration. Similarly, we have illustrated the variation of the complex amplitude's magnitude with α in Fig. 1(b). The magnitude sets the radius of the limit cycle in the system, and from Fig. 1(b) it is evident that variation in the radius is possible by changing the cross-diffusion coefficient solely. As the wave number within the BF instability regime decreases towards the onset of BF instability point in Fig. 1(a), the magnitude increases gradually in Fig. 1(b). A decline in the magnitude with a rise in the wave number is observed outside the instability regime.

V. CONCENTRATION DYNAMICS OF THE SYSTEM

We can have both Hopf instability and traveling waves within the same parametric regime of the control parameter ν, depending on whether the selected wave number is zero or finite nonzero. The temporal pattern in a reaction-diffusion system can be traced at the critical wave number of Hopf instability from the corresponding amplitude. The evolution equation of the concentration representing the uniform oscillation near the onset of Hopf instability can be written by exploiting the amplitude equation formalism as

$$z_{IH} = z_{I0} + A_H U_{cH} \exp(i f_{cH} t) + C.C., \tag{54}$$

with z_{I0} being the time-independent uniform base state for the extended direction and A_H being the amplitude part within the oscillatory regime given by Eq. (34).

The evolution equation of the concentration, z_{ITW}, representing traveling waves near the onset of Hopf instability have expression similar to the Hopf instability. However, unlike the Hopf instability, the amplitude part A_H holds the spatial variation in the case of traveling waves owing to the nonzero wave number. Hence the final general form of concentration dynamics within the oscillatory regime is given by

$$\begin{pmatrix} x \\ y \end{pmatrix} = \begin{pmatrix} x_0 \\ y_0 \end{pmatrix} + \sqrt{\lambda - q^2} \begin{pmatrix} 2\cos(\omega_0 t + f_{cH} t + qr) + 2\sin(\omega_0 t + f_{cH} t + qr) \\ -2\cos(\omega_0 t + f_{cH} t + qr) \end{pmatrix}. \tag{55}$$

It is important to note here that the cross diffusion in a two-variable reaction-diffusion model can generate diffusion-driven Turing instability in the system [37,38]. However, we have not considered Turing instability in this report. The spatiotemporal chaos can also emerge for large system sizes in the presence of cross diffusion [39]. This chaotic behavior is also out of the scope of this study. The concentration dynamics in Eq. (55) only captures the dynamic features of Hopf instability and traveling waves within the parametric regime of interest. For the nonequilibrium thermodynamic study of the

spatiotemporal pattern in the presence of cross diffusion due to overlapping of Turing and Hopf instability, one can consult Ref. [40].

VI. THERMODYNAMICS OF NONLINEAR PHENOMENON OF CHEMICAL REACTION NETWORK

The nonequilibrium thermodynamic framework of nonlinear dynamic phenomena [41,42] at steady state can generate the system's energetics near the onset of Hopf instability for uniform oscillation and a traveling waves pattern. The thermodynamic description of the pattern would reveal more about controlling the system's pattern and performance through diffusion coefficients around the BF instability and parametric phase-reversal dynamics.

A. Conservation laws and emergent cycles

The stoichiometric matrix of the reversible Selkov model in Eq. (11) is

$$S_\rho^\sigma = \begin{array}{c} \\ S \\ P \\ A \\ B \end{array} \begin{array}{c} \begin{array}{ccc} R_1 & R_2 & R_3 \end{array} \\ \begin{pmatrix} 1 & -1 & 0 \\ 0 & 1 & -1 \\ -1 & 0 & 0 \\ 0 & 0 & 1 \end{pmatrix} \end{array} \tag{56}$$

The left null vectors corresponding to the left null space of the stoichiometric matrix S_ρ^σ are defined as the conservation laws [43] and can be obtained from the expression

$$\sum_\sigma l_\sigma^\lambda S_\rho^\sigma = 0, \tag{57}$$

where

$$\{l_\sigma^\lambda\} \in \mathbb{R}^{(\sigma - w)\times\sigma}, \quad w = rank(S_\rho^\sigma).$$

For the stoichiometric matrix Eq. (56) of the reversible Selkov model, the conservation law of the closed reaction network is

$$l_\sigma^{\lambda=1} = \begin{array}{c} \begin{array}{cccc} X & Y & A & B \end{array} \\ \begin{pmatrix} 1 & 1 & 1 & 1 \end{pmatrix} \end{array}.$$

Components [43], conserved quantities of the chemical reaction network, are defined as

$$L_\lambda = \sum_\sigma l_\sigma^\lambda z_\sigma \tag{58}$$

such that $\frac{d}{dt}\int dr L_\lambda = 0$. Thus the component corresponding to the conservation law is $L_1 = s + p + a + b$. The conservation law of the system, $l_\sigma^{\lambda=1}$, is broken as the system is opened by chemostatting. Therefore, the corresponding component of the open system is no longer a global conserved quantity. The right null space of the stoichiometric matrix, $S_\rho^\sigma c_\sigma^n$, represents the internal cycle. However, this chemical reaction network has no internal cycle. The right null eigenvector corresponding to null space of S_ρ^I is defined as the emergent cycle [44]. States of intermediate species remain unchanged over a complete emergent cycle, but chemostatted species are exchanged between the system and chemostats. The total number of chemostatted species is equal to the sum of the number of broken conservation laws and the number of emergent cycles in the open chemical reaction network [41,44]. Therefore, the reversible Selkov model has one independent emergent cycle:

$$c_1 = \begin{array}{c} \begin{array}{cc} 1 & 1 \end{array} \\ \begin{array}{c} 2 \\ 3 \end{array} \begin{pmatrix} 1 \\ 1 \end{pmatrix} \end{array}.$$

B. Entropy production rate

The forward or reverse flux corresponding to an elementary reaction can be expressed in accord with mass action law by $j_{\pm\rho} = k_{\pm\rho}\prod_\sigma z_\sigma^{v_{\pm\rho}^\sigma}$, with $'+'$ and $'-'$ the labels for the forward and backward reactions, respectively, and $v_{\pm\rho}^\sigma$ denotes the number of molecules of a particular species $'\sigma'$. Thus the net flux will be $j_\rho = j_{+\rho} - j_{-\rho}$. The thermodynamic driving forces of the reaction known as reaction affinities [45] is given by $f_\rho = -\sum_\sigma S_\rho^\sigma \mu_\sigma$, where $S_\rho^\sigma = v_{-\rho}^\sigma - v_{+\rho}^\sigma$ is the stoichiometric coefficient of species and $\mu_\sigma = \mu_\sigma^o + \ln\frac{z_\sigma}{z_0}$ is the chemical potential with solvent concentration z_0 and standard-state chemical potential μ_σ^o. The nonequilibrium concentrations of intermediate species solely attribute to the global nonequilibrium state of the chemical reaction network. Hence implementing the equilibrium form of thermodynamic variables in this nonequilibrium framework can be justified under the assumption that the nonequilibrium system is kept at local thermal equilibrium at a temperature set by the solvent in a dilute solution. The system is fixed at constant absolute temperature T by the solvent, and RT is considered as unity here. From the expression of affinities one can further write another form in terms of the reaction fluxes of the chemical steps as $f_\rho = \ln\frac{j_{+\rho}}{j_{-\rho}}$. Therefore the entropy production rate (EPR) due to the chemical reaction using the flux-force relation is

$$\frac{d\Sigma_R}{dt} = \frac{1}{T}\int dr \sum_\rho (j_{+\rho} - j_{-\rho}) \ln\frac{j_{+\rho}}{j_{-\rho}}. \tag{59}$$

Now, considering diffusive flux and affinity, the entropy production rate due to diffusion can be expressed as

$$\frac{d\Sigma_D}{dt} = \int dr \left[D_{11}\frac{\left\|\frac{\partial x}{\partial r}\right\|^2}{x} + D_{22}\frac{\left\|\frac{\partial y}{\partial r}\right\|^2}{y} + D_{12}\frac{\left\|\frac{\partial y}{\partial r}\right\|\left\|\frac{\partial x}{\partial r}\right\|}{x} + D_{21}\frac{\left\|\frac{\partial x}{\partial r}\right\|\left\|\frac{\partial x}{\partial r}\right\|}{y}\right]. \tag{60}$$

The last two terms on the right in Eq. (60) represent the contribution of the cross diffusion of the intermediate species.

Total EPR comprises the homogeneous part EPR, reaction EPR, and diffusion EPR. Under the second law of thermodynamics, the total EPR will always be positive.

C. Semigrand Gibbs free energy

We need to take the open system's true thermodynamic potentials to analyze the chemical reaction network's energetics at the nonequilibrium regime. The nonequilibrium Gibbs free energy of a reaction network can be expressed in terms of the chemical potential as [46]

$$G = G_0 + \sum_{\sigma\neq 0}(z_\sigma\mu_\sigma - z_\sigma), \tag{61}$$

with $G_0 = z_0\mu_0^o$. However, to capture the energetics of the open system properly one needs to define the semigrand Gibbs free energy [42] of the system analogous to the grand potential of the grand-canonical ensemble. The semigrand Gibbs free energy of an open system can be acquired by operating a Legendre transformation [41] on the nonequilibrium Gibbs free energy,

$$\mathcal{G} = G - \sum_{\lambda_b} \mu_{\lambda_b} M_{\lambda_b}, \tag{62}$$

where $M_{\lambda_b} = \sum_{C_b} l_{C_b}^{\lambda_b{}^{-1}} L_{\lambda_b}$ represents moieties exchanged between chemostats and the system. Now the affinities acting along emergent cycles of the system obey the following equation,

$$\mu_\epsilon = c_\epsilon \ln \frac{k_\rho}{k_{-\rho}} z_c^{-S_\rho^c}, \tag{63}$$

where z_c and S_ρ^c are respectively the concentrations and stoichiometric elements corresponding to the chemostatted species.

VII. RESULTS AND DISCUSSION

The intermediate species' concentration dynamics are considered in a simple 1D glycolysis model in the regime of Hopf instability for uniform oscillation and traveling waves. Its direct correspondence in the evolution of the entities carrying the entropic and energetic descriptions of the system far from the equilibrium has been investigated systematically. All the figures here correspond to a NESS in a one-dimensional system of length $l = 200$ with absolute temperature $T = 300$ K, diffusion coefficients $D_{11} = D_{22} = 0.000\,51$, $D_{12} = -0.0002$, $D_{21} = 0.0002$, and for weakly reversible reactions, i.e., chemical reaction rate constants $k_{-\rho} = 10^{-4}$ unless otherwise indicated. Here, forward reaction rate constants of Eq. (11) are considered as $k_1 = k_2 = 1$ and $k_3 = 2$. As both theoretical [47] and experimental [48] evidence regarding temperature dependence of glycolysis oscillation are available, one should stick to a constant temperature assumption. A constant temperature assumption implies heat diffuses much faster than the intermediate species of the reaction-diffusion model. For the parameter $\omega = 2$, we would have a self-sustained oscillation for the regime below ν_{cH}. As a further expansion of the parameter space of ν results in an unphysical negative concentration of Y with other parameter values used in this analysis, we have deliberately chosen a comparatively small parametric space in the vicinity of ν_{cH} for Hopf instability. Moreover, implementing CGLE as the backbone of our analytical investigation restricts us to near the onset of instability. We have used here discrete wave numbers for all the analysis regarding traveling waves due to the finite domain with periodic boundary conditions as discussed in detail in Sec. IV B.

Initially, the system is at a uniform base state set by steady-state values of two intermediate species. We have used a time step of 0.16 and have considered 520 grid points for a system size of $l = 200$. Concentration profiles of the intermediate species over the system length in Fig. 3 for a range of control parameter values are obtained at a NESS using the analytical evolution equation of concentrations, Eq. (55). The total entropy production in Fig. 6 is acquired using Eqs. (59) and (60) with the aid of concentrations of species at NESS. Similarly, the semigrand Gibbs profiles in Fig. 7 are obtained from Eq. (62).

In the lower panel of Fig. 2, we have illustrated the dynamics of the real part of the amplitude field A_H in normalized form near the Hopf instability regime. The dynamics of A_H are obtained from Eq. (34) (i.e., Z in the equation) with the aid of Eqs. (35a) and (35b). Therefore the variation of the real part of A_H reflects dynamical features of both the phase and magnitude. In the upper panel of Fig. 2, variation of the phase ϕ with the control parameter is demonstrated by using Eq. (42). Now for the Hopf instability in Fig. 2(d), the selected wave number is simply zero, and we can observe an irregular oscillatory behavior of the real part of the Hopf amplitude field A_H for a NESS at time $t = 400$ as the control parameter ν is varied within the Hopf instability regime. The Hopf amplitude's different magnitude concerning the control parameter implies how the corresponding limit cycle's radius gets modified. This amplitude profile helps us to understand the dynamics of local concentration in the Hopf instability parameter space at a fundamental level. Figure 2(a) shows the system's phase change for the Hopf instability as a function of the control parameter. The comparison between Figs. 2(d) and 2(a) suggests that corresponding to a "double-well-shaped" region of low amplitude at $\nu = 2.5$ in Fig. 2(d), the phase of the system passes through a local minimum. Therefore we can state that the appearance of the double-well-shaped, low-amplitude region in the normalized amplitude profile is due to phase minima at that point in the case of Hopf instability. Now for traveling waves, initial changes in the normalized profile are mainly due to quantization of the wave number (see Fig. 5). One can notice no notable change in the normalized real part of the amplitude field of Fig. 2(e) while phase passes through the minimum in Fig. 2(b). However, when the spatial distribution of the system phase ceases to a single point in Fig. 2(b), a spatially homogeneous part in the normalized amplitude in Fig. 2(e) appears near $\nu = 2.6$. In Figs. 2(d) and 2(e), we can also observe that the magnitude exhibits a gradual increase relatively far from the onset of oscillatory instability point for the variation of the control parameter. The phase and amplitude change for traveling waves in the limit of infinite size, i.e., for continuous wave number bands, are illustrated in Figs. 2(c) and 2(f), respectively. Both the phase and amplitude of the traveling waves with continuous wave numbers exhibit more smooth transitions than their discrete wave-number counterparts.

The three-dimensional (3D) concentration field and a corresponding image of the intermediate species X as obtained from the analytical Eq. (55) are presented in Fig. 3. One can notice an extra-wide region of low concentration between the control parameter value $\nu = 2.4$ and $\nu = 2.6$ in Fig. 3(d). The extra wide region of low concentration has a one-to-one correspondence with the double-well-shaped low amplitude. We also discussed that the low-amplitude profile is connected with the phase slope sign change from negative to positive. To understand the wide low-concentration region area in terms of the amplitude equation coefficients, we need to consider Fig. 4(a). The red dotted line of Fig. 4(a) corresponds to the

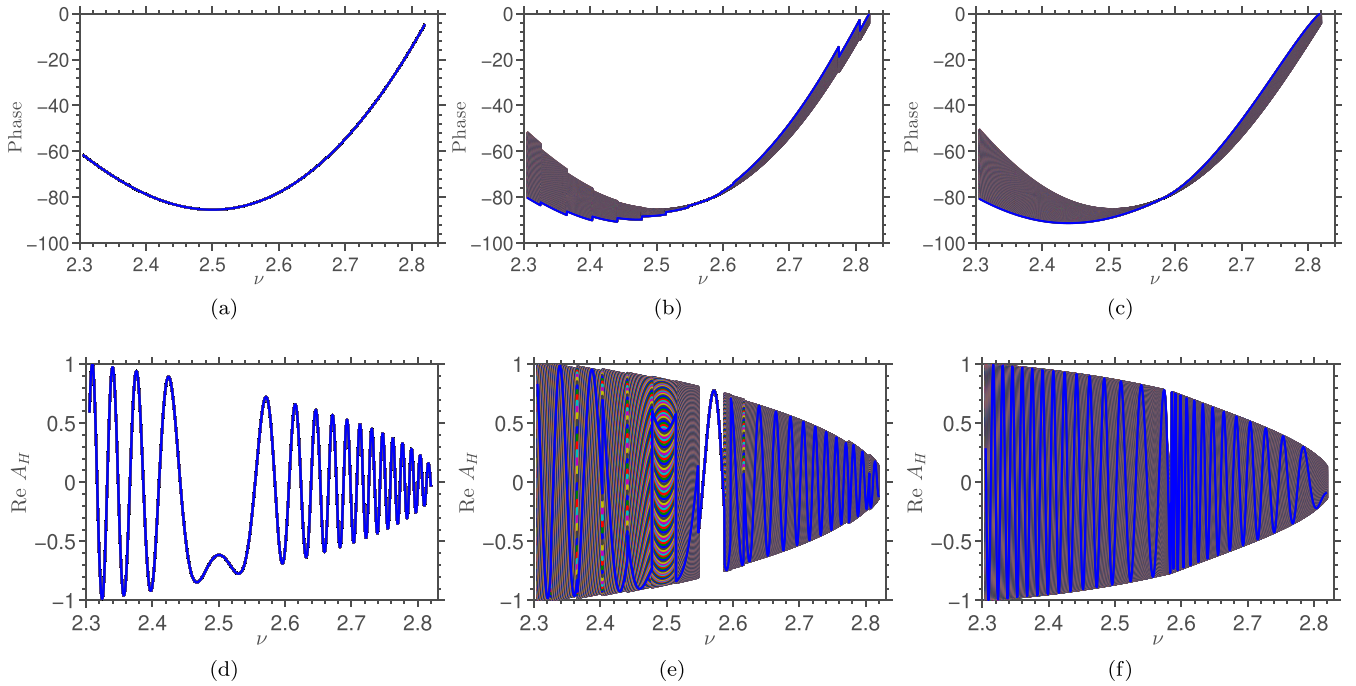

FIG. 2. The system's phase as a function of the control parameter ν is illustrated in Figs. 2(a) and 2(b) for Hopf instability and traveling waves, respectively, for finite domain of length $l = 200$. The phase change in the limit of infinite size is illustrated in Fig. 2(c). The normalized real part of the Hopf amplitude denoted by Re A_H comprised of magnitude and phase is obtained analytically as a function of control parameter ν at time $t = 400$ in Fig. 2(d). The corresponding normalized real part of amplitude fields for traveling waves for discrete and continuous wave number are shown in Figs. 2(e) and 2(f), respectively. These amplitude figures will provide a better understanding of the local concentration profile in the 1D Selkov model in the parameter space of Hopf instability and traveling waves. Here the diffusion coefficients are $D_{11} = D_{22} = 0.00051$, $D_{12} = -0.0002$, $D_{21} = 0.0002$, and the value of the parameter ω is set as 2.

variation $\alpha + \beta$ of the CGLE with control parameter ν, and the dotted black line refers to $\alpha + \beta = 0$ or $1 - \alpha\beta = 0$ condition. As discussed in Sec. IV A, whenever the $\alpha + \beta$ values cross the $\alpha + \beta = 0$ line, the phase of the spiral is reversed. However, the $\alpha + \beta$ profile always remains below the zero line in Fig. 4(a). Here the solid blue line in Fig. 4(a) represents the $1 - \alpha\beta$ condition. The $1 - \alpha\beta$ profile crosses the zero line near $\nu = 2.6$ and signals a transition from the uniform oscillation to BF instability with the control parameter variation. Now one can notice that the amplitude in Fig. 2(d) demonstrates an abrupt low-amplitude profile before the point of onset of BF instability, and this low-amplitude profile dictates the extra wide low-concentration region of the concentration field shown in Fig. 3(d). As the control parameter value is increased beyond the onset of instability point, there is a damped oscillation type of behavior. Moreover, corresponding to the extra wide low-concentration regime in the X concentration of the Hopf instability, we can observe a clear turn back before moving towards the center in the illustration, similar to a phase portrait in Fig. 4(b). Therefore the direction change in the phase portrait of the Hopf instability is a consequence of a phase slope sign at the fundamental level. Lavrova et al. [23] found a pulsating regime in temporal dynamics of X concentration within the uniform oscillatory regime corresponding to phase reversal with time in a previous study of glycolytic wave propagation with inhomogeneous substrate influx.

Instead of the zero wave number of uniform oscillation, when we consider a small finite wave number near $q_{cH} = 0$, we would obtain a traveling-wave-type concentration profile within the oscillatory regime of the system. In Fig. 5, the wave number near the critical wave number of the Hopf instability is shown as a function of the externally controlled parameter ν. Discrete wave numbers for different control parameter values that have been used as allowed wave numbers for the traveling wave can be seen from the bold line in Fig. 5. These discrete values of wave number are allowed in the finite domain with periodic boundary conditions and are obtained with the aid of the analytically derived continuous wave number expressions, Eqs. (51) and (53). The wave number decreases and approaches the critical value of wave number for Hopf instability as we change the control parameter value towards the onset of the BF instability point while all other parameters remain constant. Then we have again considered discrete and finite wave numbers within the BF instability region. In the same figure, a dashed line shows the corresponding continuous wave number profile, which can be selected as valid wave numbers in the limit of infinite system size. The 3D concentration field of X for the traveling waves with discrete wave numbers is shown in Fig. 3(b) and the corresponding image of the concentration field are presented in Fig. 3(e). In the stable oscillatory regime of the control parameter, traveling waves are demonstrated for discrete wave numbers within the linearly stable wave number limit in Fig. 3(e). Even when the control parameter goes beyond the onset of BF instability, as seen in Fig. 4(a), our selection of nonzero wave number generates a modulated pattern due to the convective nature of BF instability as seen in Fig. 3(e). The disconnectedness

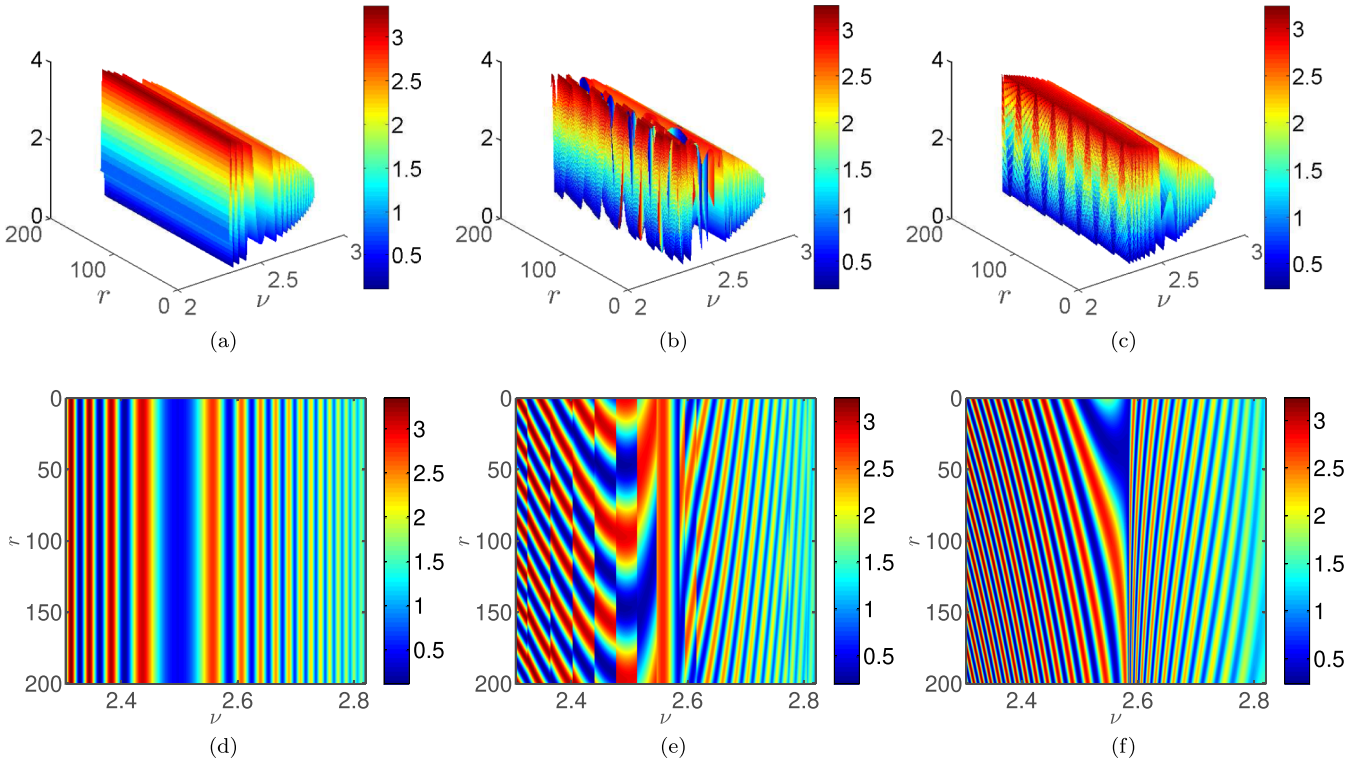

FIG. 3. In Fig. 3(a), the 3D concentration field of X for the Hopf instability in the Selkov model of length $l = 200$ as a function of the externally controlled parameter ν is presented (plot of Y is similar) at time $t = 400$ and temperature $T = 300$ K for a fixed value of parameter $\omega = 2$. The "jet" color map is used to show contrast in concentration field. Figure 3(d) illustrates the corresponding image of the concentration field of X. The 3D concentration field of X for the same system in the case of traveling waves with finite system consideration is illustrated in Fig. 3(b) and the corresponding image is shown in Fig. 3(e). The extended spatial dimension is considered along the vertical axis. The 3D concentration field of X and corresponding image for traveling waves with a continuous family of wave numbers in the limit of infinite size are demonstrated in Figs. 3(c) and 3(f), respectively. Diffusion coefficients are $D_{11} = D_{22} = 0.00051$, $D_{12} = -0.0002$, $D_{21} = 0.0002$, and all the reactions are weakly reversible, i.e., $K_{-\rho} = 10^{-4}$.

in the traveling wave pattern is due to the different discrete wave number values corresponding to the control parameter values. Modification in the traveling waves pattern around the BF instability due to the control parameter variation is dictated by the change in amplitude dynamics while passing through the onset of the BF instability point. For traveling waves, by selecting the zero wave number around the onset of BF instability as seen from Fig. 5, amplitude dynamics have a spatially homogeneous part in Fig. 2. Although the wave number of the traveling waves at the onset of BF instability

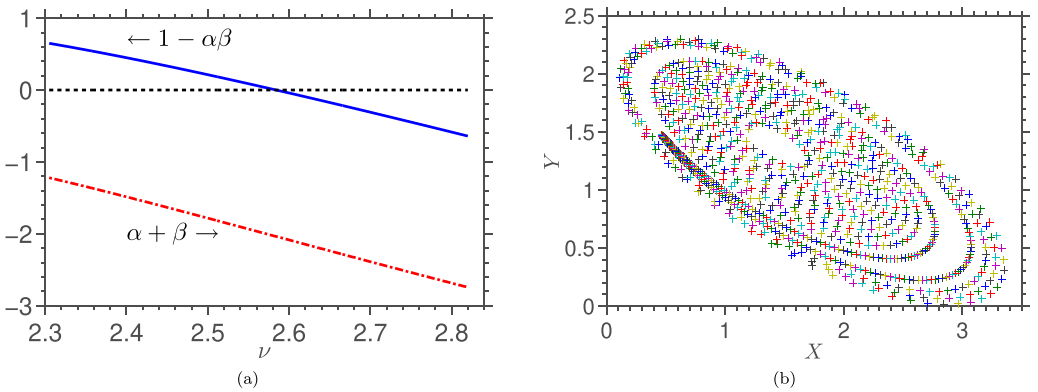

FIG. 4. The Benjamin-Feir (BF) instability and phase-reversal defining conditions corresponding to the amplitude equation are shown in Fig. 4(a). Figure 4(b) illustrates a plot similar to a phase portrait in the case of Hopf instability. Here X and Y concentrations dynamics are obtained by varying ν but for a fixed time $t = 400$. The red dotted line in Fig. 4(a) corresponds to $\alpha + \beta$ and the solid blue line represents $1 - \alpha\beta$. As the $1 - \alpha\beta$ line crosses the zero line (the dotted black line), we enter the BF instability regime. Diffusion coefficients are $D_{11} = D_{22} = 0.000\,51$, $D_{12} = -0.0002$, $D_{21} = 0.0002$, and all the reactions are weakly reversible, i.e., $K_{-\rho} = 10^{-4}$.

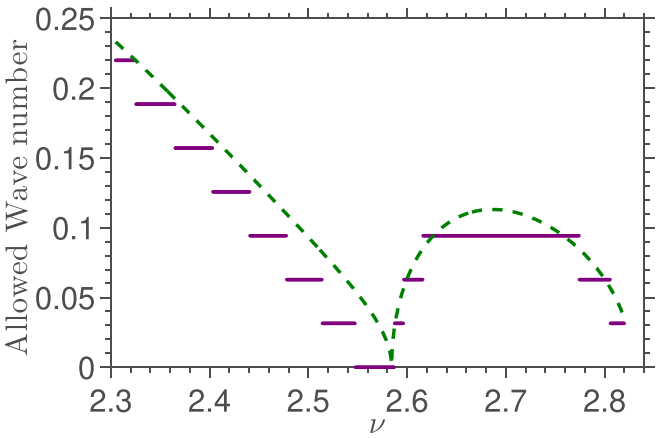

FIG. 5. The wave number near the onset of Hopf instability. For the finite system of length $l = 200$, we have shown discrete allowed values of wave number below the continuous wave number. The continuous wave number in the limit of infinite size is illustrated by the dashed line. Here the diffusion coefficients are $D_{11} = D_{22} = 0.00051$, $D_{12} = -0.0002$, $D_{21} = 0.0002$, and the value of the parameter ω is set as 2.

is equal to the Hopf instability wave number, we need to treat them as two different dynamic features. For the infinite size limit, wave numbers of traveling waves can have continuous values, as shown in Fig. 5. For continuous wave number, the concentration pattern of traveling waves is different from its finite domain counterpart. The 3D concentration field of X and the corresponding image of the concentration field for the infinite size limit are shown in Figs. 3(c) and 3(f), respectively. The difference in the concentration pattern of intermediate species for the discrete wave numbers and the continuous wave numbers is predictable given their different amplitude dynamics. Therefore, by incorporating the idea of different instability conditions directly related to amplitude equation coefficients α and β with the amplitude dynamics concerning ν in 2, we can understand and predict the profiles in Fig. 3 better. The α parameter playing an important role in setting instability conditions in the amplitude framework contains both the self and cross-diffusion coefficients. Thus the cross diffusion can alone shift the parametric regimes shown in Fig. 4(a) and thus modify the temporal concentration pattern to a significant extent, especially in the case of equal self-diffusion coefficients.

The entropy production rate owing to its origin to reaction and diffusion in the system is obtained separately using Eqs. (59) and (60), respectively, in the presence of cross diffusion. Even in the traveling wave case where the wave number selection directly depends on the parameter containing diffusion coefficients, there is no significant contribution from the diffusion part to the entropy production. Therefore total entropy production is basically due to the sum of the initial homogeneous part and reaction dynamics of the global system.

We have investigated the total EPR response due to the variation in the control parameter ν, keeping another parameter ω constant in both the Hopf and traveling wave cases. For Hopf instability, a nonzero total EPR shows oscillatory response, as shown in Fig. 6(a). Comparing profiles of the global concentration of X and Y in Fig. 6(d) and corresponding total EPR in Fig. 6(a), one observes that the total EPR is quantitatively proportional to the global concentration of Y. Moreover, they have qualitatively similar dynamics. In other words, the total EPR reflects the global dynamics of Y concentration. This similarity implies that we can exploit the total EPR of a dissipative system as a quantitative and qualitative measure of the system's temporal pattern. The traveling wave total EPR in Fig. 6(b) exhibits a pulse-type response around the onset of BF instability point. The total EPR of traveling waves otherwise shows a clear upward trend against the control parameter as seen in Fig. 6(b). The oscillatory nature of traveling waves is not prominent for discrete wave number cases. The total EPR of traveling waves in the limit of infinite system size exhibits the oscillatory nature of traveling waves over the whole range of ν and only suffers an abrupt sharp change around the onset point of BF instability. Similar to the Hopf instability, the total EPR of the traveling wave is analogous to the global dynamics of Y concentration in Figs. 6(e) and 6(f). Thus a dissipative system's total EPR can capture the temporal and spatial inhomogeneities both quantitatively and qualitatively, irrespective of its size.

Figure 7(a) illustrates the semigrand Gibbs free energy change as a function of the control parameter ν for Hopf instability. As suggested by Fig. 7(a), semigrand Gibbs free energy oscillates around its unstable homogeneous counterpart. The semigrand Gibbs free energy has a $(2:1)$ periodic oscillation feature. The extra wide low-concentration regime of X concentration field can also be identified at around $\nu = 2.5$ as a comparatively slow change in the semigrand Gibbs free energy profile. The plot of slopes for the same thermodynamic entity is shown in Fig. 7(d), and as expected it confirms the slow variation of semigrand Gibbs free energy at around $\nu = 2.5$. For traveling waves in a finite domain with periodic boundary conditions, the semigrand Gibbs free energy against ν is demonstrated in Fig. 7(b), and corresponding slopes are shown in Fig. 7(e). Like the total entropy production rate, the oscillatory behavior of traveling waves with discrete wave number is not clear enough in the energetic entity. However, the change in the semigrand Gibbs free energy due to the spatial pattern generation is visible as it separates the semigrand Gibbs free energy profile of the traveling wave from the unstable homogeneous counterpart. The semigrand Gibbs free energy for the traveling wave is greater than the system's unstable homogeneous counterpart except for around the onset of the BF instability point. The increase in semigrand Gibbs free energy for the spatial pattern is due to the work needed to vary the wave number of the traveling wave. Around the onset of BF instability point, the wave number of a traveling wave for finite system size is equal to the critical wave number to Hopf instability, and the semigrand Gibbs free energy decreases from its value for the unstable homogeneous state and passes through a minimum. Unlike the discrete wave number case, the semigrand Gibbs free energy in the infinite size limit has a prominent oscillatory behavior and exhibits a clear maximum at the onset of BF instability.

Slopes of semigrand Gibbs free energy in the Hopf instability and traveling waves are of the same order in Fig. 7. Akin to the total entropy production rate, a pulselike behavior appears

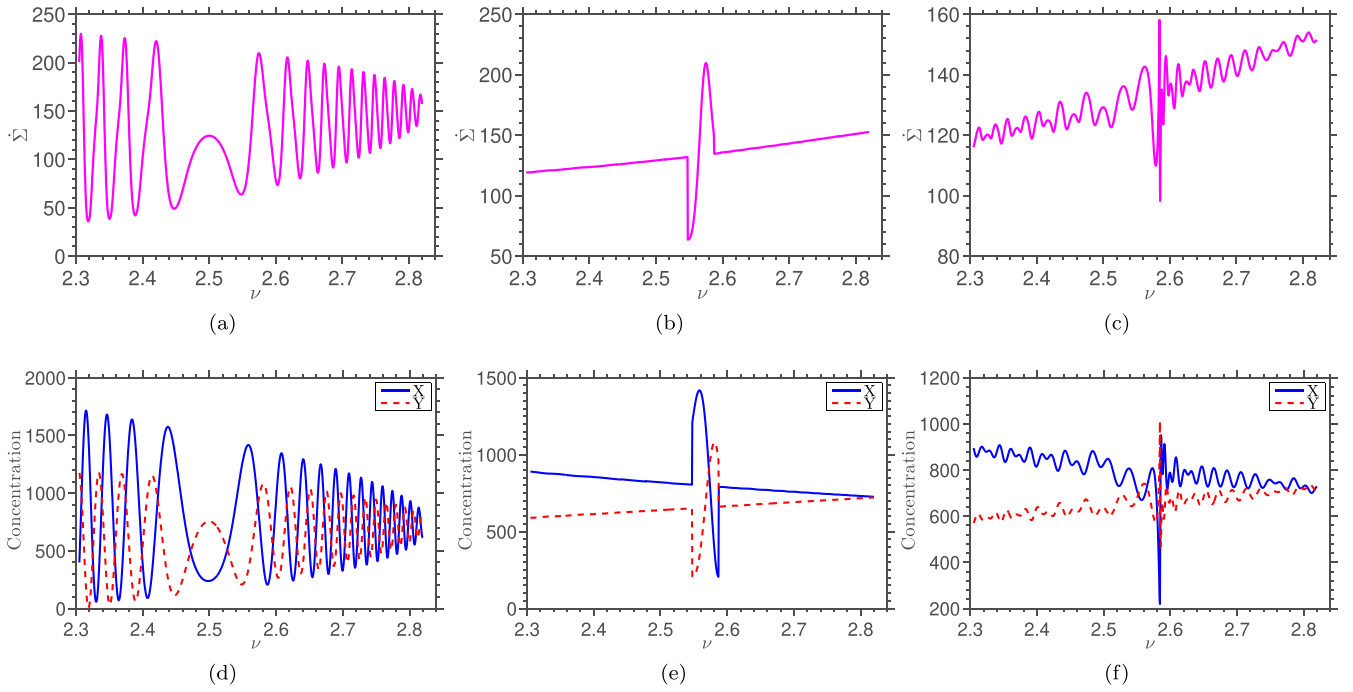

FIG. 6. Total entropy production of Hopf instability with respect to control parameter ν is obtained analytically for a 1D Selkov model of length $l = 200$ at time $t = 400$ and absolute temperature, $T = 300$ K for $\omega = 2$. Total entropy production rate is comprised of entropy production rates due to the homogeneous part and reaction part. Global concentration fields of intermediate species X and Y as a function of ν are presented in Fig. 6(d). Total entropy production of traveling waves of the same system with discrete wave numbers is presented in Fig. 6(b). In the case of traveling waves, global concentration fields of intermediate species X and Y vs control parameter are shown in Fig. 6(e). In the limit of infinite size, the total entropy production rate and global concentration fields of intermediate species of traveling waves are presented in Figs. 6(c) and 6(f). It is very apparent from Figs. 6(a) and 6(d) and Figs. 6(b) and 6(e) that entropy production rate is proportional to global concentration of Y in terms of both magnitude and phase. For all the cases the diffusion coefficients are $D_{11} = D_{22} = 0.000\,51$, $D_{12} = -0.0002$, $D_{21} = 0.0002$, and elementary chemical reactions are weakly reversible, i.e., $K_{-\rho} = 10^{-4}$.

around the onset of BF instability in the slope of semigrand Gibbs free energy for the finite system size in Fig. 7(e). A close similarity in the profiles of entropy production rate and slope of the semigrand Gibbs free energy is also observed for the infinite size limit, as shown in Fig. 7(f). These similarities suggest that the slope of the semigrand Gibbs free energy is proportional to the total entropy production rate of the system.

VIII. CONCLUSION

Capturing the uniform oscillation and traveling wave dynamics of the system are implemented here by a CGLE-based description to a more general reaction-diffusion system in the presence of cross diffusion. Then opting for a rigorous nonequilibrium framework for entropic and energetic characterization of the temporal and spatial dynamics of the system, we have provided a general recipe for relating any dynamic signature with nonequilibrium thermodynamic entities explicitly. Besides the uniform oscillation and traveling waves, this analytical study applies to any pattern or overlapping of different patterns [49–51] within a more general environment or the spatiotemporal dynamics owing to BF instability.

As the amplitude equation explicitly contains all the diffusion matrix elements, diffusion coefficients affect the amplitude and phase of the system through the form of a CGLE solution. Besides, the wave number also has implicit cross-diffusion dependence, which is again reflected by the coefficients of the amplitude equation. Here the challenging task of wave number selection in the nonequilibrium system has been handled by obtaining a boundary value of linearly stable wave number through the perturbation method of testing the stability of plane waves and then modifying it for the finite domain case by considering admissible discrete wave number values.

We have restricted ourselves to the global thermodynamic description of Hopf instability and traveling waves in this report. As all conservation laws of the closed system are broken here by chemostatting in the corresponding open system, the semigrand Gibbs free energy is equivalent to the system's energetic entity at the local level [52]. Our previous study [40] found the proportionality of the total EPR with the global concentration profile in the Turing-Hopf overlapping regime. Here, we have obtained that EPR dynamics is analogous to the global concentration dynamics, both qualitatively and quantitatively, for uniform oscillation and traveling waves. We have also acquired a pulselike shape in the total EPR profile at the onset of BF instability for the finite wave numbers. However, in the limit of infinite system size with continuous wave number, the total EPR profile demonstrates a sharp change at the onset of BF instability.

We have found that the energetics of the Hopf instability over the whole control parameter range is more complicated than the traveling wave. Here the appearance of a $(2:1)$ periodic oscillation in semigrand Gibbs free energy of the Hopf

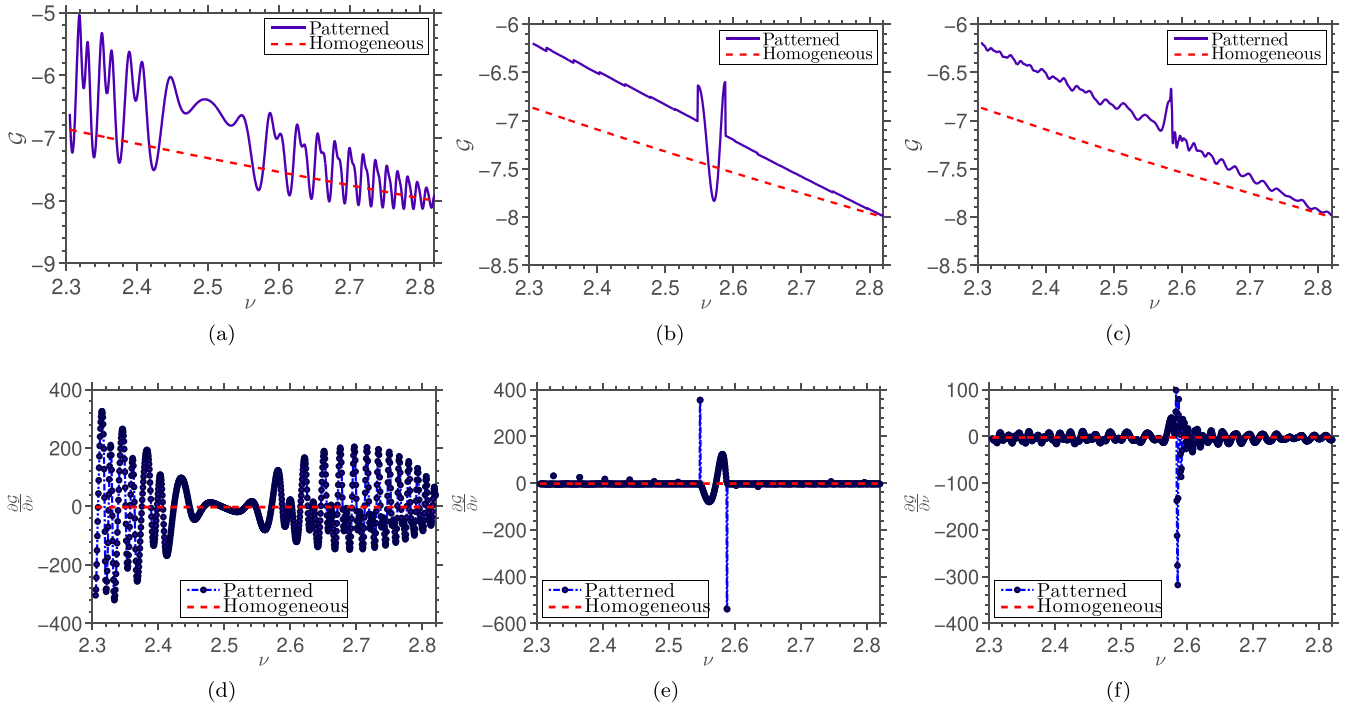

FIG. 7. The semigrand Gibbs free energy and corresponding slope of the Hopf instability are illustrated in Figs. 7(a) and 7(d), respectively, as functions of the control parameter ν at $t = 400$ and $T = 300$ K for fixed parameter $\omega = 2$. The same entities for traveling waves of discrete wave numbers are presented in Figs. 7(b) and 7(e), respectively. In the limit of infinite size, the semigrand Gibbs free energy and corresponding slope profile of traveling waves are shown in Figs. 7(c) and 7(f), respectively. The dotted lines are for the unstable homogeneous state of the system in both cases. For all the cases diffusion coefficients are $D_{11} = D_{22} = 0.000\,51$, $D_{12} = -0.0002$, $D_{21} = -0.0002$.

instability is an example of nonlinear resonance. Surprisingly, we have obtained different natures of the semigrand Gibbs free energy around the BF onset associated with discrete and continuous wave number consideration. This contradiction indicates the significance of considering the finite boundary effect for a thorough investigation of the traveling wave in a real situation.

Here we have considered sufficiently small but equal self-diffusion coefficients [16,23,53] in the presence of a cross-diffusion coefficient to generate complex oscillation patterns. The thermodynamic description of Hopf instability and the traveling wave can be extended to control the collective dynamics of biological, physical, or chemical oscillators from a new perspective [54]. It is also possible to extend this analysis to study the spiral waves [55] and their phase-reversal scenario [56–58]. We believe this CGLE-based framework can be applied even in the super- or subdiffusive regime as well as in the presence of concentration-dependent diffusion. However, it is noteworthy that CGLE may be questionable [59] to capture the antiwave-to-wave transition, as the transition can happen away from the Hopf onset point. In a similar context, the thermodynamic framework for the nonelementary chemical reaction network [60] is also relevant.

[1] J. D. Murray, *Interdisciplinary Applied Mathematics* (Springer, New York, 2003), Vol. 2, p. 838.

[2] I. R. Epstein and J. A. Pojman, *An Introduction to Nonlinear Chemical Dynamics: Oscillations, Waves, Patterns, and Chaos* (Oxford University Press, Oxford, England, 1998).

[3] M. Cross and H. Greenside, *Pattern Formation and Dynamics in Nonequilibrium Systems* (Cambridge University Press, Cambridge, England, 2009).

[4] A. Goldbeter, *Biochemical Oscillations and Cellular Rhythms: The Molecular Bases of Periodic and Chaotic Behaviour* (Cambridge University Press, Cambridge, England, 1997).

[5] M. Falcke, Reading the patterns in living cells—The physics of Ca^{2+} signaling, Adv. Phys. **53**, 255 (2004).

[6] K. Thurley, A. Skupin, R. Thul, and M. Falcke, Fundamental properties of Ca^{2+} signals, Biochim. Biophys. Acta, Gen. Subj. **1820**, 1185 (2012).

[7] L. F. Olsen, M. J. B. Hauser, and U. Kummer, Mechanism of protection of peroxidase activity by oscillatory dynamics, Eur. J. Biochem. **270**, 2796 (2003).

[8] A. Ghosh and B. Chance, Oscillations of glycolytic intermediates in yeast cells, Biochem. Biophys. Res. Commun. **16**, 174 (1964).

[9] A. Boiteux, A. Goldbeter, and B. Hess, Control of oscillating glycolysis of yeast by stochastic, periodic, and steady source of substrate: A model and experimental study, Proc. Natl. Acad. Sci. **72**, 3829 (1975).

[10] E. E. SEL'KOV, Self-oscillations in glycolysis 1. A simple kinetic model, Eur. J. Biochem. **4**, 79 (1968).
[11] A. Goldbeter, Patterns of spatiotemporal organization in an allosteric enzyme model, Proc. Natl. Acad. Sci. **70**, 3255 (1973).
[12] F. Hynne, S. Danø, and P. Sørensen, Full-scale model of glycolysis in saccharomyces cerevisiae, Biophys. Chem. **94**, 121 (2001).
[13] J. Wolf and R. Heinrich, Effect of cellular interaction on glycolytic oscillations in yeast: A theoretical investigation, Biochem. J. **345**, 321 (2000).
[14] M. F. Madsen, S. Danø, and P. G. Sørensen, On the mechanisms of glycolytic oscillations in yeast, FEBS J. **272**, 2648 (2005).
[15] S. Bagyan, T. Mair, Y. Suchorski, M. J. B. Hauser, and R. Straube, Spatial desynchronization of glycolytic waves as revealed by Karhunen-Loève analysis, J. Phys. Chem. B **112**, 14334 (2008).
[16] A. I. Lavrova, L. Schimansky-Geier, and E. B. Postnikov, Phase reversal in the Selkov model with inhomogeneous influx, Phys. Rev. E **79**, 057102 (2009).
[17] H. Qian, Open-system nonequilibrium steady state: Statistical thermodynamics, fluctuations, and chemical oscillations, J. Phys. Chem. B **110**, 15063 (2006).
[18] T. Mair and S. C. Müller, Traveling NADH and proton waves during oscillatory glycolysis in vitro, J. Biol. Chem. **271**, 627 (1996).
[19] S. Bagyan, T. Mair, E. Dulos, J. Boissonade, P. De Kepper, and S. C. Müller, Glycolytic oscillations and waves in an open spatial reactor: Impact of feedback regulation of phosphofructokinase, Biophys. Chem. **116**, 67 (2005).
[20] I. S. Aranson and L. Kramer, The world of the complex Ginzburg-Landau equation, Rev. Mod. Phys. **74**, 99 (2002).
[21] R. Straube, S. Vermeer, E. M. Nicola, and T. Mair, Inward rotating spiral waves in glycolysis, Biophys. J. **99**, L4 (2010).
[22] R. Straube and E. M. Nicola, Diffusive coupling can discriminate between similar reaction mechanisms in an allosteric enzyme system, BMC Syst. Biol. **4**, 165 (2010).
[23] A. Lavrova, S. Bagyan, T. Mair, M. Hauser, and L. Schimansky-Geier, Modeling of glycolytic wave propagation in an open spatial reactor with inhomogeneous substrate influx, Biosystems **97**, 127 (2009).
[24] D. V. Verveyko, A. Y. Verisokin, and E. B. Postnikov, Mathematical model of chaotic oscillations and oscillatory entrainment in glycolysis originated from periodic substrate supply, Chaos **27**, 083104 (2017).
[25] H. R. Petty, Spatiotemporal chemical dynamics in living cells: From information trafficking to cell physiology, Biosystems **83**, 217 (2006).
[26] M. Behar and A. Hoffmann, Understanding the temporal codes of intra-cellular signals, Curr. Opin. Genet. Dev. **20**, 684 (2010).
[27] J. E. Purvis and G. Lahav, Encoding and decoding cellular information through signaling dynamics, Cell **152**, 945 (2013).
[28] V. K. Vanag and I. R. Epstein, Cross-diffusion and pattern formation in reaction-diffusion systems, Phys. Chem. Chem. Phys. **11**, 897 (2009).
[29] P. H. Richter, P. Rehmus, and J. Ross, Control and dissipation in oscillatory chemical engines, Prog. Theor. Phys. **66**, 385 (1981).
[30] N. M. Krylov and N. N. Bogoliubov, *Introduction to Non-Linear Mechanics* (Princeton University Press, Princeton, NJ, 1949).
[31] S. Ghosh and D. S. Ray, Chemical oscillator as a generalized Rayleigh oscillator, J. Chem. Phys. **139**, 164112 (2013).
[32] J. W. S. Rayleigh and R. B. Lindsay, *The Theory of Sound* (Dover, New York, 1945).
[33] G. Nicolis, *Introduction to Nonlinear Science* (Cambridge University Press, Cambridge, England, 1995), p. 254.
[34] D. Walgraef, The Hopf bifurcation and related spatio-temporal patterns, in *Spatio-Temporal Pattern Formation* (Springer, New York, 1997), pp. 65–85.
[35] T. B. Benjamin, Instability of periodic wavetrains in nonlinear dispersive systems, Proc. R. Soc. London, Series A **299**, 59 (1967).
[36] R. Hoyle, *Pattern Formation: An Introduction to Methods* (Cambridge University Press, Cambridge, England, 2006).
[37] G. Gambino, M. Lombardo, and M. Sammartino, Pattern formation driven by cross-diffusion in a 2D domain, Nonlinear Anal. Real World Appl. **14**, 1755 (2013).
[38] J. M. Chung and E. Peacock-López, Bifurcation diagrams and turing patterns in a chemical self-replicating reaction-diffusion system with cross diffusion, J. Chem. Phys. **127**, 174903 (2007).
[39] I. Berenstein and C. Beta, Spatiotemporal chaos arising from standing waves in a reaction-diffusion system with cross-diffusion, J. Chem. Phys. **136**, 034903 (2012).
[40] P. Kumar and G. Gangopadhyay, Energetic and entropic cost due to overlapping of Turing-Hopf instabilities in the presence of cross diffusion, Phys. Rev. E **101**, 042204 (2020).
[41] R. Rao and M. Esposito, Nonequilibrium Thermodynamics of Chemical Reaction Networks: Wisdom from Stochastic Thermodynamics, Phys. Rev. X **6**, 041064 (2016).
[42] G. Falasco, R. Rao, and M. Esposito, Information Thermodynamics of Turing Patterns, Phys. Rev. Lett. **121**, 108301 (2018).
[43] R. A. Alberty, *Thermodynamics of Biochemical Reactions* (John Wiley & Sons, Inc., Hoboken, NJ, 2003).
[44] M. Polettini and M. Esposito, Irreversible thermodynamics of open chemical networks. I. Emergent cycles and broken conservation laws, J. Chem. Phys. **141**, 024117 (2014).
[45] I. Prigogine, *Chemical Thermodynamics* (Longmans, London, 1954).
[46] E. Fermi, *Thermodynamics* (Dover Publications, New York, 1956), p. 160.
[47] E. B. Postnikov, D. V. Verveyko, and A. Y. Verisokin, Simple model for temperature control of glycolytic oscillations, Phys. Rev. E **83**, 062901 (2011).
[48] T. Mair, C. Warnke, K. Tsuji, and S. C. Muüller, Control of glycolytic oscillations by temperature, Biophys. J. **88**, 639 (2005).
[49] A. De Wit, D. Lima, G. Dewel, and P. Borckmans, Spatiotemporal dynamics near a codimension-two point, Phys. Rev. E **54**, 261 (1996).
[50] W. Just, M. Bose, S. Bose, H. Engel, and E. Schöll, Spatiotemporal dynamics near a supercritical Turing-Hopf bifurcation in a two-dimensional reaction-diffusion system, Phys. Rev. E **64**, 026219 (2001).
[51] L. Yang and I. R. Epstein, Oscillatory Turing Patterns in Reaction-Diffusion Systems with Two Coupled Layers, Phys. Rev. Lett. **90**, 178303 (2003).
[52] F. Avanzini, G. Falasco, and M. Esposito, Thermodynamics of chemical waves, J. Chem. Phys. **151**, 234103 (2019).
[53] A. Y. Verisokin, D. V. Verveyko, and E. B. Postnikov, Traveling glycolytic waves induced by a temperature gradient and

determination of diffusivities for dense media, Phys. Rev. E **86**, 012901 (2012).

[54] D. M. Abrams and S. H. Strogatz, Chimera States for Coupled Oscillators, Phys. Rev. Lett. **93**, 174102 (2004).

[55] A. T. Winfree, Spiral waves of chemical activity, Science **175**, 634 (1972).

[56] V. K. Vanag and I. R. Epstein, Inwardly rotating spiral waves in a reaction-diffusion system, Science **294**, 835 (2001).

[57] Y. Gong and D. J. Christini, Antispiral Waves in Reaction-Diffusion Systems, Phys. Rev. Lett. **90**, 088302 (2003).

[58] T.-C. Li and B.-W. Li, Reversal of spiral waves in an oscillatory system caused by an inhomogeneity, Chaos **23**, 033130 (2013).

[59] X. Shao, Y. Wu, J. Zhang, H. Wang, and Q. Ouyang, Inward Propagating Chemical Waves in a Single-Phase Reaction-Diffusion System, Phys. Rev. Lett. **100**, 198304 (2008).

[60] F. Avanzini, G. Falasco, and M. Esposito, Thermodynamics of non-elementary chemical reaction networks, New J. Phys. **22**, 093040 (2020).